# An extended Prandtl solution for analytical modelling of the bearing capacity of a shallow foundation on a spatially variable undrained clay

J.H. Li[1], C.L. Wu[1], W.Z. Luo[1], L.W. Sun[1], and D. White[2*]

1. Department of Civil and Environmental Engineering, Harbin Institute of Technology (Shenzhen), 518055, China

2. National Infrastructure Laboratory, University of Southampton, Burgess Road, Southampton, SO16 7QF, UK

*Corresponding author, Email: david.white@soton.ac.uk

## ABSTRACT

Classical bearing capacity theory was developed mainly based on spatially uniform soil properties, which cannot account for the influence of inherent soil variability. If the soil strength is heterogenous, then using the average strength may overestimate the bearing capacity of foundations, because the failure mechanism may preferentially mobilise the weaker soils. This study aims to establish a theoretical model using upper-bound solutions applied to the bearing capacity analysis of shallow foundations on undrained clay considering spatial variability. The model is derived on the principle of least energy dissipation using a four-parameter variation on Prandtl's mechanism. The developed theoretical model is verified by the random finite element method in spatially-varying soil conditions. The results show that the model can accurately capture the effect of spatially-varying strength on the shallow foundation failure mechanism. The difference of bearing capacity factor between the proposed model and the FE model is within 5%, which demonstrates that the four-parameter model has an accuracy that is comparable to finite element analysis with many hundreds of degrees of freedom. Another advantage of the theoretical model is that the possible non-convergence in finite element analysis can be avoided, and hence, the calculation efficiency is significantly enhanced. The model is therefore suitable for rapid quantification of bearing capacity in spatially-varying soils.

**KEYWORDS**: shallow foundation; bearing capacity factor; spatial variability; theoretical model; energy dissipation

# INTRODUCTION

The bearing capacity of a shallow foundation under vertical loading is a classical geotechnical problem. Several theoretical models for the bearing capacity of shallow foundations have been proposed. Prandtl (1920) first proposed an analytical solution for the shear failure mechanism using a limit equilibrium method, ignoring soil weight and the burial depth of a shallow foundation. Many well-known scholars (Terzaghi, 1965; Meyerhof, 1951; Hansen, 1970; Vesić, 1973) subsequently revised the Prandtl model to account for variable situations in estimating bearing capacity. Key early contributions by Hill (1950) and Drucker and Prager (1952) established limit theorems of plasticity combining the lower bound methods based on a static stress field and the upper bound methods based on work done via a velocity field, which are now widely adopted in geotechnical engineering (e.g., Chen, 1975; Davis and Selvadurai, 2002; Knappett and Craig, 2012; Sloan, 2013). Solutions for shallow foundations involve a symmetrical shear failure mechanism in uniform soils (see Fig. 1). According to the upper bound theorem of limit analysis techniques, the work done by external loads and the energy dissipation by internal stresses in an increment of displacement can be respectively expressed as

$$E_{\mathrm{w}} = V_{\mathrm{ult}} \cdot v \tag{1}$$

$$E_{\mathrm{h}} = \sum S_a \cdot l_a \cdot v_a \tag{2}$$

where $E_{\mathrm{w}}$ is the work done rate (per unit thickness) acting on the foundation soil, $E_{\mathrm{h}}$ is the energy dissipation rate (per unit thickness) in a homogeneous soil acting along a shear failure plane. $V_{\mathrm{ult}}$ is the ultimate vertical bearing capacity (per unit thickness), $v$ is the known vertical velocity of the shallow foundation, $S_a$ is the undrained shear strength along shear failure plane $a$, $l_a$ is the length of plane $a$, and $v_a$ is the slip velocity on that plane.

For a homogeneous soil, the undrained shear strength is the same everywhere. A bearing capacity factor of a shallow foundation on the homogeneous soil ($N_{\mathrm{h}}$) is often defined as

$$N_{\mathrm{h}} = \frac{V_{\mathrm{ult}}}{W \cdot S_a} \tag{3}$$

where $W$ is the width of the shallow foundation. According to the equation for the work shown in Eq. (1), the bearing capacity factor can be alternatively expressed as

$$N_{\mathrm{h}} = \frac{E_{\mathrm{w}}}{v \cdot W \cdot S_a} \tag{4}$$

If a kinematically admissible velocity field is postulated, the energy dissipation rate is equal to the work done rate (i.e., $E_{\mathrm{h}} = E_{\mathrm{w}}$), and it can be derived that,

$$N_{\mathrm{h}} = \frac{E_{\mathrm{h}}}{v \cdot W \cdot S_a} \tag{5}$$

The same bearing capacity factor as the Prandtl solution of 5.14 under undrained conditions in a homogeneous soil can be obtained using Eqs. (2) and (5).

The previous theoretical results are mainly limited to homogeneous soils or uniform soils of strength increasing linearly with depth. However, soil is a natural material and shows variations in properties from point to point in the ground as a result of inherent variations in composition during formation. Lumb (1966) reported that the undrained strength of Hong Kong marine clay varied with depth. An autocorrelation function for the spatial series of depth versus undrained strength was recommended to study the correlation structure of the undrained strength (Matsuo and Asaoka, 1977; Asaoka and Grivas, 1982). The spatial variability of the undrained strength of clay was then characterized by various researchers (Chiasson et al., 1995; Dasaka and Zhang, 2012; Houlsby and Houlsby, 2013; Lloret-Cabot et al., 2014). This variability may cause a reduction of the bearing capacity and the shear failure mechanism tends to follow the weakest path (Griffiths and Fenton, 2001; Griffiths et al., 2002; Fenton and Griffiths, 2003; Popescu et al., 2005; Cho and Park, 2010; Li et al., 2015). This effect is overlooked if the bearing capacity is calculated using the conventional bearing capacity factor combined with the spatial average value of the soil strength. The bearing capacity can therefore be overestimated if the inherent spatial variability of a soil is ignored.

Vanmarcke and Fenton (Vanmarcke, 1977; Fenton and Vanmarcke, 1990) presented random field theory for modeling the natural variability of soil properties. Then, random finite element method (RFEM) was developed by combining random field theory and finite element method, which provides a rational framework for the analysis of complex uncertain problems (Griffiths and Fenton, 1997). Griffiths and Fenton (2001) investigated the influence of the spatial variability of the undrained soil strength on the bearing capacity by combining elasto-plastic finite element analysis with random field theory. They found that the mean bearing capacity of a shallow foundation can decrease by 20% for spatially variable soils compared with that of homogeneous soils. Griffiths & Fenton (2001) and Popescu et al. (2005) showed that the shear failure mechanism tends to pass through the weaker soil zones. Li et al. (2015) quantified this effect by showing the correlation between shear plane length and variability of bearing capacity in spatially-variable soils. Although the RFEM shows its capability on tackling with this problem, it is complex due to the tedious modeling process, high requirements on computing resources and tough convergence conditions. A theoretical model that can describe the bearing capacity on spatially variable soils is required.

This study establishes a theoretical model using upper-bound solutions applied to the bearing capacity analysis of shallow foundations on spatially variable soils. The proposed theoretical model is verified by the classical bearing capacity theory in homogeneous soils and by random finite element method in spatially variable soils. It is the first time that a simple theoretical analysis for bearing capacity problem in spatially variable soils has been proposed. The analysis provides insights into the influence of spatial heterogeneity and provides a practical tool for the quantification of these effects for specific heterogeneity conditions.

# THEORETICAL MODEL

### *Kinematically admissible velocity field*

According to the Prandtl solution in homogeneous soils, there is a key point below the shallow foundation that controls the geometry of the failure plane, which is marked in Fig. 1 as point C. This point is the base of a triangular zone originating from the center of the foundation, which is marked as point $O_1$. The angle ACB is a right angle for undrained soil. The shear failure mechanism for the shallow foundation is symmetric about a vertical plane through $O_1$. The classical bearing capacity solution features three zones with different velocity fields and energy dissipation patterns, which include a wedge zone (triangle ACB), a radial shear zone (fan ACD and fan BCF) and a passive zone (triangle ADE and triangle BFG).

When considering the spatial variability of the soil, the shear failure mechanism tends to become asymmetric (Griffiths and Fenton, 2001). The key point C is no longer beneath the midpoint of the foundation as shown in Fig. 2, and lies below the point marked as O'. The location of point C is controlled by the zones of weak soil beneath. In turn, the angle ACB is not necessarily 90°as in the homogeneous soil case.

As a result, the angle CAB ($\theta_3$) and CBA ($\theta_4$) can be different under this condition. The development of the shear failure plane in spatially variable soils is significantly affected by the spatial pattern of soils, which may lead to different angles of CAD ($\theta_1$) and CBF ($\theta_2$). Although the angles may change, the failure plane still contains three zones including the wedge zone (triangle ACB), radial shear zone (fan ACD and fan BCF) and passive zone (triangle ADE and triangle BFG).

To allow for this potential asymmetry, we now set out a derivation of a generalized version of Prandtl's solution, with variables angles $\theta_1$ and $\theta_2$. The foundation is regarded as a rigid body with a vertical downward velocity of $v$. The three zones will move accordingly. The energy dissipates along the sliding lines AC, BC, DE, FG and around the perimeter of the sliding fans ACD and BCF. It is noted that, the energy also dissipates within the fans ACD and BCF due to internal shearing. A potential failure mechanism for the spatially variable soil is shown in Fig. 3a, where the fan ACD (or fan BCF) is simplified to a cluster of infinitesimal wedges. In order to achieve compatibility, the velocity is uniform along each radial line, including the boundaries with the wedge zone. A kinematically admissible velocity field for the failure mechanism is postulated to define the relative velocities between each shear failure plane and the stationary soil mass, which is shown in Fig. 3b. Each infinitesimal wedge slips relative to the adjacent wedges with the velocity shown in Fig. 3c.

The velocity of point C is $v$ as the area surrounded by triangle ACB is assumed to be rigid. The slip velocity of the soil along the shear failure plane AC ($v_{AC}$) is closely related with the velocity of point C,

$$v_{\mathrm{AC}} = v \cdot \sin\theta_3 \tag{6}$$

$$\sin\theta_3 = \frac{l_{\mathrm{CO'}}}{l_{\mathrm{AC}}} \tag{7}$$

$$l_{CO'} = y_0 - y \tag{8}$$

$$l_{AC} = \sqrt{\left[\frac{W}{2} + (x - x_0)\right]^2 + (y - y_0)^2} \tag{9}$$

where $l_{\mathrm{CO'}}$ is the length of line CO', $l_{\mathrm{AC}}$ is the length of line AC, ($x$, $y$) are the coordinates of point C, and ($x_0$, $y_0$) are the coordinates of point $O_1$.

Similarly, the slip velocity of the soil along the shear failure plane BC ($v_{\mathrm{BC}}$) is

$$v_{\mathrm{BC}} = v \cdot \sin\theta_4 \tag{10}$$

$$\sin\theta_4 = \frac{l_{\mathrm{CO'}}}{l_{\mathrm{BC}}} \tag{11}$$

$$l_{\mathrm{BC}} = \sqrt{\left[\frac{W}{2} - (x - x_0)\right]^2 + (y - y_0)^2} \tag{12}$$

where $l_{\mathrm{BC}}$ is the length of line BC.

The shear failure plane CD is a circular arc for ease of calculation. The slip velocity of the soil along the shear failure plane CD ($v_{\mathrm{CD}}$) is perpendicular to line AC at point C originally. As we move along arc CD, it changes direction until it is perpendicular to line AD at point D, but keeps values unchanged throughout which can be derived from the hodograph shown in Fig. 3b,

$$v_{\mathrm{CD}} = v \cdot \cos\theta_3 \tag{13}$$

$$\cos\theta_3 = \frac{l_{\mathrm{AO'}}}{l_{\mathrm{AC}}} \tag{14}$$

$$l_{AO'} = \frac{W}{2} + (x - x_0) \tag{15}$$

where $l_{\mathrm{AO'}}$ is the length of line AO'.

Similarly, the slip velocity of the soil along the shear failure plane CF ($v_{\mathrm{CF}}$) is

$$v_{\mathrm{CF}} = v \cdot \cos\theta_4 \tag{16}$$

$$\cos\theta_4 = \frac{l_{\mathrm{BO'}}}{l_{\mathrm{BC}}} \tag{17}$$

$$l_{\mathrm{BO'}} = \frac{W}{2} - \left(x - x_0\right) \tag{18}$$

where $l_{\mathrm{BO'}}$ is the length of line BO'.

The area surrounded by triangle ADE and triangle BFG is rigid. Hence the slip velocity of the soil along the shear failure plane DE (or FG) is equal to that of the shear failure plane CD (or CF) (see Fig. 3b). The mechanism leads to a kinematically admissible velocity field which includes the following shear failure planes between the soil zones,

$$\begin{cases} v_{\mathrm{AC}} = v \cdot \dfrac{y_0 - y}{\sqrt{\left[\dfrac{W}{2} + \left(x - x_0\right)\right]^2 + \left(y - y_0\right)^2}} \\ v_{\mathrm{CD}} = v_{\mathrm{DE}} = v \cdot \dfrac{\dfrac{W}{2} + \left(x - x_0\right)}{\sqrt{\left[\dfrac{W}{2} + \left(x - x_0\right)\right]^2 + \left(y - y_0\right)^2}} \\ v_{\mathrm{BC}} = v \cdot \dfrac{y_0 - y}{\sqrt{\left[\dfrac{W}{2} - \left(x - x_0\right)\right]^2 + \left(y - y_0\right)^2}} \\ v_{\mathrm{CF}} = v_{\mathrm{FG}} = v \cdot \dfrac{\dfrac{W}{2} - \left(x - x_0\right)}{\sqrt{\left[\dfrac{W}{2} - \left(x - x_0\right)\right]^2 + \left(y - y_0\right)^2}} \end{cases} \tag{19}$$

The above shear failure mechanism is an extension of the classical Prandtl solution that adds variation associated with the position of point C, and the angles $\theta_1$ and $\theta_2$. This simple variation turns out to be sufficient to capture a wide range of failure patterns that optimize the collapse load in spatially variable soil, as shown later.

***Energy dissipation***

The shear failure mechanism for the shallow foundation is closely related to the spatial distribution of the soil strength. For a certain site, the shear failure mechanism will follow the path with the minimum energy dissipation. In order to determine the minimum energy dissipation, the site is considered as a combination of discrete elements and the undrained shear strength of these elements is regarded as a random field (as shown in Fig. 4).

According to Eq. (2), the energy dissipation rate in a spatially variable soil ($E_s$) can be expressed as

$$E_{\mathrm{s}} = \sum_{i=1}^{m} S_i \cdot l_i \cdot v_i \tag{20}$$

where $m$ is the number of the elements along the shear failure planes, namely the number of the elements that are crossed by the shear failure planes, $S_i$ is the undrained shear strength of the element $i$ along the shear failure plane, $l_i$ is the length of the part of the shear failure plane which is in element $i$, and $v_i$ is the slip velocity of the element $i$ along the shear failure plane. The energy dissipation rate in each zone is derived in the following sections.

The wedge zone of triangle ACB has two shear failure planes (i.e., line AC and line BC), which generates two sources of energy dissipation,

$$\begin{cases} E_{\mathrm{AC}} = \sum_{j=1}^{m1} S_{\mathrm{AC}(j)} \cdot l_j \cdot v_{\mathrm{AC}} \\ E_{\mathrm{BC}} = \sum_{k=1}^{m2} S_{\mathrm{BC}(k)} \cdot l_k \cdot v_{\mathrm{BC}} \end{cases} \tag{21}$$

where $E_{AC}$ is the energy dissipation rate in the soil elements acting along plane AC, $m1$ is the number of the elements along plane AC, $S_{AC(j)}$ is the undrained shear strength of element $j$ along plane AC, $l_j$ is the length of the part of plane AC which is in element $j$, $E_{\mathrm{BC}}$ is the energy dissipation rate in the soil elements acting along plane BC, $m2$ is the number of the elements along plane BC, $S_{\mathrm{BC}(k)}$ is the undrained shear strength of the element $k$ along plane BC, and $l_k$ is the length of the part of plane BC which is in element $k$.

The radial shear zone contains two sliding fans (i.e., fan ACD and fan BCF). Each sliding fan has two sources of energy dissipation. Taking fan ACD as an example, the first source is the energy dissipation of the soil elements located in fan ACD due to the slip on the radial planes between adjacent soil elements. The energy dissipation rate in the soil elements located in fan ACD ($E_{\mathrm{ACD}}$) is the summation of the energy dissipation due to the shearing occurring between the infinitesimal wedges (see Figs. 3a and 3c),

$$E_{\mathrm{ACD}} = \sum_{i'=1}^{m'} E_{\mathrm{WEDGE}(i')} \tag{22}$$

$$E_{\mathrm{WEDGE}(i')} = \sum_{j'=1}^{n'} S_{\mathrm{ACD}(i',j')} \cdot l_{(i',j')} \cdot \left(v_{\mathrm{CD}} \delta\theta_1\right) \tag{23}$$

where $m'$ is the number of the infinitesimal wedges, $E_{\mathrm{WEDGE}(i')}$ is the energy dissipation rate occurring between wedge $i'$ and the next one, $n'$ is the number of the elements along the contact plane between wedge $i'$ and the next, $S_{\mathrm{ACD}(i',j')}$ is the undrained shear strength of the element $j'$ along the contact plane between wedge $i'$ and the next, $l_{(i',j')}$ is the length of the part of the contact plane between wedge $i'$ and the next which is in element $j'$, and $\delta\theta_1$ is the internal angle of the infinitesimal wedge from the segmentation of angle $\theta_1$ (see Fig. 3).

As the energy dissipation occurring between each wedge and its next is similar throughout the fan, Eqs. (22) and (23) can be combined and further simplified as

$$E_{\mathrm{ACD}} = \sum_{l=1}^{m3} S_{\mathrm{ACD}(l)} \cdot l_l \cdot \left(v_{\mathrm{CD}} \delta\theta_1\right) \tag{24}$$

where $m3$ is the total number of the elements along the contact planes between these wedges, $S_{\mathrm{ACD}(l)}$ is the undrained shear strength of the element $l$ along the contact planes between two wedges, and $l_l$ is the length of the part of the contact plane between two wedges which is in element $l$.

The other source of energy dissipation in fan ACD is from the shearing along plane CD ($E_{\mathrm{CD}}$), which can be expressed as

$$E_{CD} = \sum_{p=1}^{m4} S_{\mathrm{CD}(p)} \cdot l_p \cdot v_{\mathrm{CD}} \tag{25}$$

where $m4$ is the number of the elements along plane CD, $S_{\mathrm{CD}(p)}$ is the undrained shear strength of the element $p$ along the plane CD, and $l_p$ is the length of the part of plane CD which is in element $p$. It is noted that the length of a line segment is the length of a circular arc here since fan ACD is discretized into the infinitesimal wedges.

As the energy dissipation in fan BCF is similar to that in fan ACD, its two components of energy dissipation can be written as

$$\begin{cases} E_{\mathrm{BCF}} = \sum_{q=1}^{m5} S_{\mathrm{BCF}(q)} \cdot l_q \cdot \left(v_{\mathrm{CF}} \delta\theta_2\right) \\ E_{\mathrm{CF}} = \sum_{r=1}^{m6} S_{\mathrm{CF}(r)} \cdot l_r \cdot v_{\mathrm{CF}} \end{cases} \tag{26}$$

where the notation follows the convention set out for Eqs. (24) and (25).

The passive zone also contains two shear failure planes (i.e., line DE and line FG), which generates two items of energy dissipation,

$$\begin{cases} E_{\mathrm{DE}} = \sum_{s=1}^{m7} S_{DE(s)} \cdot l_s \cdot v_{DE} \\ E_{\mathrm{FG}} = \sum_{t=1}^{m8} S_{FG(t)} \cdot l_t \cdot v_{FG} \end{cases} \tag{27}$$

where the notation follows the convention set out for Eq. (21).

***Bearing capacity factor***

When the energy dissipation in the wedge zone, radial shear zones and passive zones are all determined, the energy dissipation rate in spatially variable soil acting along a potential shear failure mechanism ($E_p$) can be expressed as

$$E_{\mathrm{p}} = E_{\mathrm{AC}} + E_{\mathrm{BC}} + E_{\mathrm{ACD}} + E_{\mathrm{CD}} + E_{\mathrm{BCF}} + E_{\mathrm{CF}} + E_{\mathrm{DE}} + E_{\mathrm{FG}} \tag{28}$$

To bound the optimization process, point C is assumed to be confined to an area that is laterally between the edges of the foundation and less than 1W vertically beneath the foundation. Trials have shown that this zone is sufficiently large to capture the optimum mechanism. The optimum and therefore critical shear failure mechanism is that with the minimum energy dissipation rate. The optimisation model can therefore be defined as:

$$\begin{cases} E_s = \min E_p \\ x_A \le x \le x_B \\ 0 < y < W \\ 0 \le \theta_1 \le \pi \\ 0 \le \theta_2 \le \pi \end{cases} \tag{29}$$

where $x_A$ is the $x$-axis coordinate of point A and $x_B$ is the $x$-axis coordinate of point B. There are four independent unknowns in Eq. (29), namely $\theta_1$, $\theta_2$, $x$, and $y$, and a numerical search program is used to satisfy this optimization for a given set of inputs.

According to Eq. (5), the bearing capacity factor of a shallow foundation on a spatially variable soil ($N_s$) can be expressed as

$$N_{\mathrm{s}} = \frac{E_{\mathrm{s}}}{v \cdot W \cdot S_{\mathrm{s}}} \tag{30}$$

where $S_s$ is the mean undrained shear strength of the spatially variable soil domain (Griffiths and Fenton, 2001).

The proposed model can be verified by the classical bearing capacity theory as the Prandtl solution in homogeneous soils can be regarded as a special case of the spatially variable field. The verification of the theoretical model is given in APPENDIX.

## SEARCH PROGRAM

It is difficult to directly obtain the analytical solutions of the energy dissipation rate and the bearing capacity of a spatially variable soil from Eqs. (29) and (30) due to the random undrained shear strength applicable to each shear failure plane and fan zone. Hence a search program written in the FORTRAN language has been developed to solve this problem.

To define the shape of the failure mechanism, point C, point E, and point G are taken as the control points (with the *x* coordinates of E and G being proxies for angles $\theta_1$ and $\theta_2$, given the location of point C). Both the angle EDA and angle GFB are constrained as right angles. Point C can be located at any positions within a designated area (e.g., 1W × 1W) beneath the foundation. Point E (or point G) can be located from the left side (or right side) of the foundation to a designated distance horizontally (e.g., 3W). Point C is tried at many positions within the designated area and for each of those positions the E and G are varied to form potential shear failure planes. Then the minimum of each of these cases is identified as the critical case for any given positions of point C. The energy dissipation rate of these potential optimum mechanisms corresponding to all potential positions of point C is calculated and the overall minimum energy dissipation is identified. The details of the above operations can be outlined as the following steps:

Step 1: Set up the input parameters including the foundation width, the dimension of the site, and the size of soil elements.

Step 2: Map the undrained shear strength of the spatially variable soil into each soil element.

Step 3: Discretize each soil element into designated small cells in which the point C can be positioned.

Step 4: Search the potential mechanisms through moving the control points (i.e., point C, point E, and point G) under the constraint conditions and calculate the energy dissipation rate along each potential mechanism based on Eq. (28).

Step 5: Record the coordinates of the control points (i.e., point C, point D, point E, point F, and point G), the number of the elements along the shear failure planes, and the undrained shear strength of these mobilised soil elements.

Step 6: Identify the shear failure mechanism with the minimum energy dissipation rate and the corresponding shear plane. Output the coordinates of the control points on the shear plane.

Step 7: Calculate the bearing capacity factor using the minimum energy dissipation rate based on Eq. (30).

The search program was first verified by confirming that it found the Prandtl solution in homogeneous soils, where all soil elements have the same undrained shear strength. The foundation width was set to 1 m. The dimension of the site is assumed to be 8 m long and 4 m deep, which is large enough to avoid any boundary effects. Three sizes of square elements (i.e., 0.5 m, 0.25 m, and 0.125 m) were simulated to investigate the effect of element size. The bearing capacity factors obtained from all of the three cases are 5.14, which is consistent with the theoretical Prandtl solution in uniform soils. The coordinates of the control point C are 4.0 m on the *x*-axis and - 0.5 m on the *y*-axis, which are the same as the Prandtl solution. The results show that the program is accurate.

## ILLUSTRATIVE EXAMPLE

An illustrative example of a shallow foundation on a spatially variable soil is presented in this section. The foundation and domain size are the same as the previous example. The spatial variability of the site is represented by a random field of undrained shear strength. The random field is considered as log-normally distributed. The mean and standard deviation of the undrained shear strength are 20 kPa and 5 kPa, respectively. A squared exponential autocorrelation function is employed to describe the spatial correlation. The scale of fluctuation in the vertical direction and the horizontal direction is taken as 1.5 m. The element size of the field should be equal to or less than 0.18 times the scale of fluctuation to represent the spatial variation (Ching and Phoon, 2013). Hence, the element size is adopted as 0.25 m, giving a mesh of 512 soil elements. One realization of the generated random field is mapped in these elements as shown in Fig. 5. To achieve a more accurate result each element was divided into 100 small cells in which the control points can be located.

The proposed theoretical model along with the search program is used to analyze the shear failure mechanism and calculate the bearing capacity factor of the shallow foundation on the spatially variable soil shown in Fig. 5. 4,000,000 potential failure planes are tried for the field. Four mechanisms therein are extracted to illustrate the potential variations in the shear failure planes as shown in Fig. 6. As can be seen, these mechanisms exhibit significant differences with each other. Among these mechanisms, the case with minimum energy dissipation is shown by the thicker black line in Fig. 6. The shear failure plane shows an asymmetric characteristic which tends to pass through the relatively weak soil. The minimum energy dissipation rate is 106.41 kJ/s. The bearing capacity factor can then be obtained using Eq. (30), which gives 5.32.

For the same statistical properties, the spatial pattern of the shear strength can be quite different. Given a lognormal undrained clay with mean strength of 20 kPa , standard deviation of 5 kPa and scale of fluctuation of 1.5 m, Monte Carlo simulations are performed involving 100 realizations of the shear strength random field and the subsequent theoretical analysis of bearing capacity. The mean value and standard deviation of the bearing capacity factor are 4.86 and 0.52, respectively.

# COMPARISON WITH RANDOM FINITE ELEMENT METHODS

## *Random finite element model*

To evaluate the accuracy of the proposed model, which is limited only to failure mechanisms of the form introduced in Fig. 2, a random finite element method (FEM) is used following the procedure set out by Li et al. (2015). The random FE approach simulates the same form of spatially random soil, but has the flexibility for a wider range of failure mechanisms to be mobilised.

The site is simulated as a two-dimensional plane-strain model. The width of the shallow foundation, the dimension of the site, the size of soil elements, and the properties of the undrained shear strength are all the same as the previous illustrative example. To ensure the numerical accuracy of the simulation, each soil element in the illustrative example is further discretized into 100 small cells which have the same undrained shear strength as their parent element.

The elastic response of soil is defined by the Young's modulus and Poisson's ratio. The Young's modulus of each soil element is assumed as 200 times the local undrained shear strength (e.g. following Lambe and Whitman, 1969). The Poisson's ratio is set slightly below 0.5 as 0.49 to simulate undrained conditions of no volume change, but avoiding mesh locking. The failure of the soil is defined following the Tresca criterion. The interface between the soil and the foundation is fully bonded. The foundation is subjected to a vertical displacement at the foundation reference point, with rotation prevented, and the vertical reaction force is calculated. The bearing capacity factor of a shallow foundation solved by the random finite element method can be obtained referring to Eq. (3).

### *Comparison of results*

For the first realization shown in illustrative example, the bearing capacity factor obtained from the random finite element method is 5.36, which is within 1% of that from the theoretical model in this study (i.e., 5.32). The bearing capacity factor for the homogeneous soil using the same FEM model is 5.21 which is 1.34% higher than the exact value of 5.14. The shear failure mechanism obtained from the FEM is shown in Fig. 7 (i.e., the grey region). The failure mechanism from the theoretical model (i.e., the black line) is also plotted on the figure for comparison purpose. In general, the failure mechanisms from the theoretical model demonstrate a similar pattern to that of the FEM. The failure plane is unsymmetrical and the identified failure mechanism tends to bypass the strong soils and develop along the weak soils, even at the expense of the shear failure planes extending further from the foundation.

The next 100 realizations with different random fields of undrained shear strength were subsequently investigated for a broader comparison. The bearing capacity factor values obtained from the theoretical model and from the FEM for each random field are compared in Fig. 8. The difference between the two methods is within 5%, which indicates the theoretical model is reasonable. 72% of the cases with spatially variable soils have a lower bearing capacity than that of the homogeneous soils. The mean value of the bearing capacity factors from the analytical model and the FEM are 4.86 and 4.95 respectively, compared to 5.14 and 5.21 for the homogeneous cases for each method respectively. These values show that the analytical method identified on average a 5.4% reduction in bearing capacity, whereas the average reduction from the FEM approach was 5.0%, which illustrates that on average there is a small effect of the mechanism 'finding' the weaker zones of soil to fail through (Griffiths and Fenton, 2001; Popescu et al., 2005; Cho and Park, 2010; Li et al., 2015). The slightly greater reduction in bearing capacity for the analytical method may attribute to the fact that the FEM method has greater flexibility in the form of the failure mechanism compared to the analytical method. The standard deviation of the bearing capacity factor is 0.52, and for this scale of fluctuation the foundation capacity is actually enhanced by the spatial variability in 28% of the cases, relative to the homogeneous strength case.

The designated ranges of the control points C, E, and G in the 100 cases were examined by expanding their range in the theoretical calculation. The searching range for point C was set to 2W x 2W beneath the foundation. The horizontal distance for searching optimal point E and point G was set as from the side of the foundation to the boundary of the soil domain (i.e., 3.5W). The coordinates of these points are shown in Fig. 9. The coordinates of point C are all lying in the range of W x W area beneath the foundation. For the range of point E and G they are all within 2W distance. Therefore, the designated search ranges are appropriate.

Regarding computation efficiency, the time used for the theoretical model is significantly less than that for the FEM, by a factor of 30. The theoretical model takes about 9.7 seconds and the FEM about 300 seconds on a computer with the CPU of 3.4 GHz and the memory of 32GB. The results show the relative advantage of the proposed model for its combination of calculation accuracy and efficiency. Moreover, the theoretical model can avoid the possible non-convergence in FEM.

## PARAMETRIC STUDIES

To investigate the general effect of spatial variability on the bearing capacity of a shallow foundation, a series of Monte Carlo simulations using 1000 realizations were performed for a range of combinations of coefficient of variation ($COV_s$) and scale of fluctuation ($SOF_s$) of the undrained shear strength. The bearing capacity factor for each realization was calculated using the proposed theoretical method. The mean value ($\mu_{Ns}$), standard deviation and coefficient of variation ($COV_{Ns}$) of the bearing capacity factor for each combination were obtained.

The variation of mean bearing capacity factor with the COV of the undrained shear strength is shown in Fig. 10a. The variation of mean bearing capacity factor with the SOF of the undrained shear strength is shown in Fig. 10b. When the variation in the undrained shear strength of soil ($COV_s$) is small the mean bearing capacity factor is close to that of the homogeneous soil (i.e., 5.14). This is because for a small COV the soil is relatively uniform. As the COV of soil strength increases the mean bearing capacity factor decreases. The large variation means that weak soils exist in the domain, and the failure mechanism adapts so that the shear plane passes through the weak soils and results in smaller energy dissipation and a lower bearing capacity factor. This trend is similar to that reported by Griffiths and Fenton (2001), although the bearing capacity factor values are not identical due to different correlation functions used in the model. A Markov spatial correlation function was used in Griffiths and Fenton (2001), and a squared exponential correlation function (Li et al., 2015) is adopted in this study. The two cases are therefore not directly comparable, and a separate question which requires further attention is the influence that different spatial correlation functions have on the bearing capacity.

The scale of fluctuation of undrained shear strength affects the mean bearing capacity as well. When the scale of fluctuation is between 0.5-2 times the foundation width the mean bearing capacity factor is the least, which is consistent with that reported by Li et al. (2016).

The coefficient of variation of the bearing capacity factor ($COV_{N\mathrm{s}}$) is significantly affected by both the COV and the scale of fluctuation of the soil strength. Fig. 11 shows that $COV_{N\mathrm{s}}$ is rather small as the scale of fluctuation is small (e.g., 0.125 times the foundation width). This is because that a small scale of fluctuation indicates that the soil strength varies intensively from a location to another. The shear plane has to go through both the weak soil and the strong soil, so the bearing capacity factor converges towards the average result. When the scale of fluctuation is very large, the $COV_{N\mathrm{s}}$ becomes large and would be identical to the coefficient of variation of soil shear strength at $SOF_{\mathrm{s}} \rightarrow \infty$. When the scale of fluctuation becomes very small, the $COV_{N\mathrm{s}}$ also becomes small and insensitive to $COV_{\mathrm{s}}$. These results show that our analytical approach can replicate the forms of behavior first highlighted by Griffiths & Fenton (2001) using the FEM, but in this study the more rapid analytical method has been used.

# CONCLUSIONS

A theoretical model is firstly proposed to describe the failure mechanism and the bearing capacity of a shallow foundation on spatially variable soils from the point view of energy dissipation. A simple four-parameter variation on Prandtl's solution is proposed to represent the asymmetrical failure mechanism in undrained clay. The energy dissipation rate is derived for the mechanism, through which the bearing capacity factor can be obtained. The developed theoretical model is carefully verified by the random finite element method in spatially variable soils. Results show that the model can accurately capture the asymmetrical failure mechanism of a foundation on spatially variable soils. The difference of bearing capacity factor between the proposed model and the FE model is within 5%, which demonstrates the proposed model is reasonable. A parametric study shows the general influence of the magnitude and length scale of strength spatial variability on bearing capacity. A notable contribution of this study is to show that a simple four-parameter variation on Prandtl's solution can capture the effect of spatially-varying strength on the shallow foundation failure mechanism, to an accuracy that is comparable to FE analysis with many hundreds of degrees of freedom.

## ACKNOWLEDGEMENTS

The authors wish to acknowledge the support of the National Natural Science Foundation of China (Grant Nos. 51979067).

## APPENDIX: VERIFICATION OF THEORETICAL MODEL

The bearing capacity factor should equal to 5.14 if the soil elements all have the same undrained shear strength,

$$\begin{aligned} &S_{\mathrm{AC}(j)} = S_{\mathrm{BC}(k)} = S_{\mathrm{ACD}(l)} = S_{\mathrm{CD}(p)} = \\ &S_{\mathrm{BCF}(q)} = S_{\mathrm{CF}(r)} = S_{\mathrm{DE}(s)} = S_{\mathrm{FG}(t)} = S_{\mathrm{s}} \end{aligned} \tag{31}$$

Combining Eq. (20) with Eq. (28), the energy dissipation rate along a potential shear failure mechanism can be reduced to

485

$$\begin{aligned}E_{\mathrm{p}} &= S_{\mathrm{s}} \cdot v_{\mathrm{AC}} \cdot \sum_{j=1}^{m1} l_j + S_{\mathrm{s}} \cdot v_{\mathrm{BC}} \cdot \sum_{k=1}^{m2} l_k \\ &+ S_{\mathrm{s}} \cdot v_{\mathrm{CD}} \cdot \sum_{l=1}^{m3} l_l \delta\theta_1 + S_{\mathrm{s}} \cdot v_{\mathrm{CD}} \cdot \sum_{p=1}^{m4} l_p \\ &+ S_{\mathrm{s}} \cdot v_{\mathrm{CF}} \cdot \sum_{q=1}^{m5} l_q \delta\theta_2 + S_{\mathrm{s}} \cdot v_{\mathrm{CF}} \cdot \sum_{r=1}^{m6} l_r \\ &+ S_{\mathrm{s}} \cdot v_{\mathrm{DE}} \cdot \sum_{s=1}^{m7} l_s + S_{\mathrm{s}} \cdot v_{\mathrm{FG}} \cdot \sum_{t=1}^{m8} l_t\end{aligned} \tag{32}$$

486 The following equation can then be obtained,

487

$$\begin{aligned}E_{\mathrm{p}} &= S_{\mathrm{s}} \cdot v_{\mathrm{AC}} \cdot l_{\mathrm{AC}} + S_{\mathrm{s}} \cdot v_{\mathrm{BC}} \cdot l_{\mathrm{BC}} \\ &+ 2S_{\mathrm{s}} \cdot v_{\mathrm{CD}} \cdot l_{\mathrm{AC}} \cdot \theta_1 \\ &+ 2S_{\mathrm{s}} \cdot v_{\mathrm{CF}} \cdot l_{\mathrm{BC}} \cdot \theta_2 \\ &+ S_{\mathrm{s}} \cdot v_{\mathrm{DE}} \cdot l_{\mathrm{DE}} + S_{\mathrm{s}} \cdot v_{\mathrm{FG}} \cdot l_{\mathrm{FG}}\end{aligned} \tag{33}$$

488 where $l_{\mathrm{DE}}$ is the length of line DE, and $l_{\mathrm{FG}}$ is the length of line FG.

489 Substituting the kinematically admissible velocity field (i.e., Eq. (19)) and the 490 length of the shear failure plane (i.e., Eq. (9) and Eq. (12)) into Eq. (33) 491 **Error! Reference source not found.** yields

$$
\begin{aligned}
E_{\mathrm{p}} = {} & S_{\mathrm{s}} \cdot v \cdot \frac{y_0 - y}{\sqrt{\left[\frac{W}{2} + \left(x - x_0\right)\right]^2 + \left(y - y_0\right)^2}} \cdot \sqrt{\left[\frac{W}{2} + \left(x - x_0\right)\right]^2 + \left(y - y_0\right)^2} \\
& + S_{\mathrm{s}} \cdot v \cdot \frac{y_0 - y}{\sqrt{\left[\frac{W}{2} - \left(x - x_0\right)\right]^2 + \left(y - y_0\right)^2}} \cdot \sqrt{\left[\frac{W}{2} - \left(x - x_0\right)\right]^2 + \left(y - y_0\right)^2} \\
& + 2S_{\mathrm{s}} \cdot v \cdot \frac{\frac{W}{2} + \left(x - x_0\right)}{\sqrt{\left[\frac{W}{2} + \left(x - x_0\right)\right]^2 + \left(y - y_0\right)^2}} \cdot \sqrt{\left[\frac{W}{2} + \left(x - x_0\right)\right]^2 + \left(y - y_0\right)^2} \cdot \theta_1 \\
& + 2S_{\mathrm{s}} \cdot v \cdot \frac{\frac{W}{2} - \left(x - x_0\right)}{\sqrt{\left[\frac{W}{2} - \left(x - x_0\right)\right]^2 + \left(y - y_0\right)^2}} \cdot \sqrt{\left[\frac{W}{2} - \left(x - x_0\right)\right]^2 + \left(y - y_0\right)^2} \cdot \theta_2 \\
& + S_{\mathrm{s}} \cdot v \cdot \frac{\frac{W}{2} + \left(x - x_0\right)}{\sqrt{\left[\frac{W}{2} + \left(x - x_0\right)\right]^2 + \left(y - y_0\right)^2}} \cdot \sqrt{\left[\frac{W}{2} + \left(x - x_0\right)\right]^2 + \left(y - y_0\right)^2} \cdot \lambda_1 \\
& + S_{\mathrm{s}} \cdot v \cdot \frac{\frac{W}{2} - \left(x - x_0\right)}{\sqrt{\left[\frac{W}{2} - \left(x - x_0\right)\right]^2 + \left(y - y_0\right)^2}} \cdot \sqrt{\left[\frac{W}{2} - \left(x - x_0\right)\right]^2 + \left(y - y_0\right)^2} \cdot \lambda_2
\end{aligned}
\tag{34}
$$

with

$$
\begin{cases}
\lambda_1 = \tan\left(\pi - \theta_1 - \arctan\dfrac{y_0 - y}{\frac{W}{2} - x_0 + x}\right) \\
\lambda_2 = \tan\left(\pi - \theta_2 - \arctan\dfrac{y_0 - y}{\frac{W}{2} + x_0 - x}\right)
\end{cases}
\tag{35}
$$

By simplifying Eq. (34), the following equation can be obtained,

$$
E_{\mathrm{p}} = S_{\mathrm{s}} \cdot v \cdot \left[2\left(y_0 - y\right) + \left(\frac{W}{2} - x_0 + x\right) \cdot \left(2\theta_1 + \lambda_1\right) + \left(\frac{W}{2} + x_0 - x\right) \cdot \left(2\theta_2 + \lambda_2\right)\right] \tag{36}
$$

When the energy dissipation rate along the potential shear failure mechanism achieves a minimum, the following equation can be obtained.

$$\begin{cases} \dfrac{\partial E_s}{\partial \theta_1} = S_s \cdot v \cdot \left[ \left( \dfrac{W}{2} - x_0 + x \right) \cdot \left( 2 - \lambda_3 \right) \right] = 0 \\ \dfrac{\partial E_s}{\partial \theta_2} = S_s \cdot v \cdot \left[ \left( \dfrac{W}{2} + x_0 - x \right) \cdot \left( 2 - \lambda_4 \right) \right] = 0 \\ \dfrac{\partial E_s}{\partial x} = S_s \cdot v \cdot \left[ 2\left( \theta_1 - \theta_2 \right) + \left( \lambda_1 - \lambda_2 \right) + \left( \dfrac{W}{2} - x_0 + x \right) \cdot \lambda_5 - \left( \dfrac{W}{2} + x_0 - x \right) \cdot \lambda_6 \right] = 0 \\ \dfrac{\partial E_s}{\partial y} = S_s \cdot v \cdot \left[ -2 + \left( \dfrac{W}{2} - x_0 + x \right) \cdot \lambda_7 + \left( \dfrac{W}{2} + x_0 - x \right) \cdot \lambda_8 \right] = 0 \end{cases} \tag{37}$$

with

$$\begin{cases} \lambda_3 = \sec^2 \left( \pi - \theta_1 - \arctan \dfrac{y_0 - y}{\dfrac{W}{2} - x_0 + x} \right) \\ \lambda_4 = \sec^2 \left( \pi - \theta_2 - \arctan \dfrac{y_0 - y}{\dfrac{W}{2} + x_0 - x} \right) \\ \lambda_5 = \lambda_3 \cdot \dfrac{y_0 - y}{\left( \dfrac{W}{2} - x_0 + x \right)^2 + \left( y_0 - y \right)^2} \\ \lambda_6 = \lambda_4 \cdot \dfrac{y_0 - y}{\left( \dfrac{W}{2} + x_0 - x \right)^2 + \left( y_0 - y \right)^2} \\ \lambda_7 = \lambda_3 \cdot \dfrac{\dfrac{W}{2} - x_0 + x}{\left( \dfrac{W}{2} - x_0 + x \right)^2 + \left( y_0 - y \right)^2} \\ \lambda_8 = \lambda_4 \cdot \dfrac{\dfrac{W}{2} + x_0 - x}{\left( \dfrac{W}{2} + x_0 - x \right)^2 + \left( y_0 - y \right)^2} \end{cases} \tag{38}$$

Solving Eq. (37)**Error! Reference source not found.**, the results are obtained as follows,

$$\begin{cases} \theta_1 = \dfrac{\pi}{2} \\ \theta_2 = \dfrac{\pi}{2} \\ x = x_0 \\ y = y_0 - \dfrac{W}{2} \end{cases} \tag{39}$$

These results are consistent with the Prandtl solution for homogeneous soils. Substituting the solution of the four unknowns into Eq. (36) **Error! Reference source not found.**, the energy dissipation rate in a spatially variable soil can be derived as

$$E_s = (2+\pi) \cdot v \cdot W \cdot S_s \tag{40}$$

Based on Eq. (30), the bearing capacity factor of a shallow foundation on a spatially variable soil can be derived as

$$N_s = \frac{(2+\pi) \cdot v \cdot W \cdot S_s}{v \cdot W \cdot S_s} \approx 5.14 \tag{41}$$

The results indicate that the coordinates of point C, the angle of CAD and CBF, as well as the bearing capacity factor obtained are all consistent with the Prandtl solution.

## NOTATION

$E_w$ work done rate acting on the foundation soil

$E_h$ energy dissipation rate in a homogeneous soil

$E_s$ energy dissipation rate in a spatially variable soil

$E_p$ energy dissipation rate in a spatially variable soil acting along a potential shear plane

$E_{AC}$ energy dissipation rate in the soil elements acting along plane AC

$E_{BC}$ energy dissipation rate in the soil elements acting along plane BC

$E_{ACD}$ energy dissipation rate in the soil elements located in fan ACD

$E_{\mathrm{BCF}}$ energy dissipation rate in the soil elements located in fan BCF

$E_{\mathrm{CD}}$ energy dissipation rate in the soil elements acting along plane CD

$E_{\mathrm{CF}}$ energy dissipation rate in the soil elements acting along plane CF

$E_{\mathrm{DE}}$ energy dissipation rate in the soil elements acting along plane DE

$E_{\mathrm{FG}}$ energy dissipation rate in the soil elements acting along plane FG

$E_{\mathrm{WEDGE}(i')}$ energy dissipation rate occurring between wedge *i*' and the next

$S_a$ undrained shear strength along shear failure plane *a*

$S_{\mathrm{s}}$ mean undrained shear strength of the spatially variable soil

$S_i$ undrained shear strength of soil element *i* along the shear failure plane

$S_{\mathrm{AC}(j)}$ undrained shear strength of element *j* along plane AC

$S_{\mathrm{BC}(k)}$ undrained shear strength of element *k* along plane BC

$S_{\mathrm{ACD}(l)}$ undrained shear strength of element *l* along the contact plane between two wedges

$S_{\mathrm{CD}(p)}$ undrained shear strength of element *p* along plane CD

$S_{\mathrm{BCF}(q)}$ undrained shear strength of element *q* along the contact plane between two wedges

$S_{\mathrm{CF}(r)}$ undrained shear strength of element *r* along plane CF

$S_{\mathrm{DE}(s)}$ undrained shear strength of element *s* along plane DE

$S_{\mathrm{FG}(t)}$ undrained shear strength of element *t* along plane FG

$S_{\mathrm{ACD}(i', j')}$ undrained shear strength of element *j*' along the contact plane between wedge *i*' and the next

$l_a$ length of shear failure plane *a*

$l_i$ length of the part of the shear failure plane which is in soil element *i*

$l_j$ length of the part of plane AC which is in element *j*

$l_k$ length of the part of plane BC which is in element *k*

$l_l$ length of the part of the contact plane between two wedges which is in element *l*

$l_p$ length of the part of plane CD which is in element *p*

$l_q$ length of the part of the contact plane between two wedges which is in element *q*

$l_r$ length of the part of plane CF which is in element *r*

$l_s$ length of the part of plane DE which is in element *s*

$l_t$ length of the part of plane FG which is in element *t*

$l_{(i', j')}$ length of the part of the contact plane between wedge $i'$ and the next which is in element $j'$

$l_{AC}$ length of line AC

$l_{BC}$ length of line BC

$l_{DE}$ length of line DE

$l_{FG}$ length of line FG

$l_{AO'}$ length of line AO'

$l_{BO'}$ length of line BO'

$l_{CO'}$ length of line CO'

$v$ vertical velocity of the shallow foundation

$v_{AC}$ slip velocity of the soil along plane AC

$v_{BC}$ slip velocity of the soil along plane BC

$v_{CD}$ slip velocity of the soil along plane CD

$v_{CF}$ slip velocity of the soil along plane CF

$v_{DE}$ slip velocity of the soil along plane DE

$v_{FG}$ slip velocity of the soil along plane FG

$v_i$ slip velocity of the soil element $i$ along the shear failure plane

$m$ number of the soil elements along the shear failure plane

$m1$ number of the soil elements along plane AC

$m2$ number of the soil elements along plane BC

$m3$ total number of the soil elements along the contact planes between the infinitesimal wedges which are located in fan ACD

$m4$ number of the soil elements along plane CD

$m5$ total number of the soil elements along the contact planes between the infinitesimal wedges which are located in fan BCF

$m6$ number of the soil elements along plane CF

$m7$ number of the soil elements along plane DE

$m8$ number of the soil elements along plane FG

$m'$ number of the infinitesimal wedges

$n'$ number of the elements along the contact plane between wedge $i'$ and the next

$\theta_1$ angle CAD

$\theta_2$ angle CBF

$\theta_3$ angle CAB

$\theta_4$ angle CBA

$\delta\theta_1$ internal angle of the infinitesimal wedge from the segmentation of angle $\theta_1$

$\delta\theta_2$ internal angle of the infinitesimal wedge from the segmentation of angle $\theta_2$

$(x, y)$ coordinates of point C

$(x_0, y_0)$ coordinates of point $O_1$

$x_A$ $x$-axis coordinate of point A

$x_B$ $x$-axis coordinate of point B

$V_{ult}$ ultimate vertical bearing capacity

$W$ width of shallow foundation

$N_h$ bearing capacity factor of a shallow foundation on a homogeneous soil

$N_s$ bearing capacity factor of a shallow foundation on a spatially variable soil

$COV_s$ coefficient of variation of the undrained shear strength

$SOF_s$ scale of fluctuation of the undrained shear strength

$\mu_{Ns}$ mean value of the bearing capacity factor

$COV_{Ns}$ coefficient of variation of the bearing capacity factor

# REFERENCES


Asaoka, A. & Grivas, D. A. (1982). Spatial variability of the undrained strength of clays. *Journal of the Geotechnical Engineering Division* **108**, No. GT5, 743-756.

Chen, W. F. (1975). *Limit analysis and soil plasticity*. New York: American Elsevier Publishing Company.

Chiasson, P., Lafleur, J., Soulié, M. & Law, K. T. (1995). Characterizing spatial variability of a clay by geostatistics. *Canadian Geotechnical Journal* **32**, No. 1, 1-10.

Ching, J. Y. & Phoon, K. K. (2013). Effect of element sizes in random field finite element simulations of soil shear strength. *Computers and Structures* **126**, 120-134.

Cho, S. E. & Park H. C. (2010). Effect of spatial variability of cross-correlated soil properties on bearing capacity of strip footing. *International Journal for Numerical and Analytical Methods in Geomechanics* **34**, No. 1, 1-26.

Dasaka, S. M. & Zhang, L. M. (2012). Spatial variability of in situ weathered soil. *Géotechnique* **62**, No. 5, 375-384.

Davis R. O. & Selvadurai A. P. S. (2002). *Plasticity and geomechanics*. Cambridge: Cambridge University Press.

Drucker, D. C. & Prager, W. (1952). Soil mechanics and plastic analysis or limit design. *Quarterly of Applied Mathematics* **10**, No. 2, 157-165.

Fenton, G. A. & Vanmarcke, E. H. (1990). Simulation of random fields via local average subdivision. *Journal of Engineering Mechanics-Asce* **116**, No. 8, 1733-1749.

Fenton, G. A. & Griffiths, D. V. (2003). Bearing-capacity prediction of spatially random c-phi soils. *Canadian Geotechnical Journal* **40**, No. 1, 54-65.

Georgiadis, K. (2010). An upper-bound solution for the undrained bearing capacity of strip footings at the top of a slope. *Géotechnique* **60**, No. 10, 801-806.

Griffiths, D. V. & Fenton, G. A. (1997). Three-dimensional seepage through spatially random soil. *Journal of Geotechnical and Geoenviromental Engineering* **123**, No. 2, 153-160.

Griffiths, D. V. & Fenton, G. A. (2001) Bearing capacity of spatially random soil: the undrained clay Prandtl problem revisited. *Géotechnique* **51**, No. 4, 351-359.

Griffiths, D. V., Fenton, G. A. & Manoharan, N. (2002). Bearing capacity of rough rigid strip footing on cohesive soil: probabilistic study. *Journal of Geotechnical and Geoenvironmental Engineering* **128**, No. 9, 743-755.

Hansen, J. B. (1970). *A revised and extended formula for bearing capacity*. Copenhagen: Geoteknisk Institute.

Hill, R. (1950) The mathematical theory of plasticity. Clarendon Press.

Houlsby, N. M. T. & Houlsby, G. T. (2013). Statistical fitting of undrained strength data. *Géotechnique* **63**, No. 14, 1253–1263.

Knappett, J. A. & Craig, R. F. (2012). *Craig's soil mechanics*, 8th edn. Abingdon: Spon Press.

Lambe T. W. & Whitman R. V. (1969). *Soil mechanics*. New York: John Wiley & Sons.

Li, J. H., Tian, Y. H. & Cassidy, M. J. (2015). Failure mechanism and bearing capacity of footings buried at various depths in spatially random soil. *Journal of Geotechnical and Geoenvironmental Engineering* **141**, No. 2, 04014099.

Li, J. H., Zhou, Y., Zhang, L. L., Tian, Y., Cassidy, M.J. & Zhang, L.M. (2016). Random finite element method for spudcan foundations in spatially variable soils. *Engineering Geology*

**205**, 146-155.

Lloret-Cabot, M., Fenton, G. A. & Hicks, M. A. (2014) On the estimation of scale of fluctuation in geostatistics. *Georisk* **8**, No. 2, 129-140.

Lumb, P. (1966). The variability of natural soils. *Canadian Geotechnical Journal* **3**, No. 2, 74-97.

Matsuo, M. & Asaoka, A. (1977). Probability models of undrained strength of marine clay layer. *Soils and Foundations* **17**, No. 3, 53-68.

Meyerhof, G. G. (1951). The ultimate bearing capacity of foudations. *Géotechnique* **2**, No. 4, 301-332.

Nobahar, A. & Popescu, R. (2000). Spatial variability of soil properties-Effects on foundation design.*Proc. 53rd Canadian Geotechnical Conference*, *Richmond*, *BC*2, 1139-1144.

Phoon, K.-K. & Kulhawy, F. H. (1999). Characterization of geotechnical variability. *Canadian Geotechnical Journal* **36**, No. 4, 612-624.

Popescu, R., Deodatis, G. & Nobahar, A. (2005). Effects of random heterogeneity of soil properties on bearing capacity. *Probabilistic Engineering Mechanics* **20**, No. 4, 324-341.

Prandtl, L. (1920). About the hardness of a plastic body. *Nachr Kgt Ges Wiss. Göttingen Math-Phys. Kl*, 74-85.

Sloan, S. W. (2013). Geotechnical stability analysis. *Géotechnique* **63**, No. 7, 531–572.

Terzaghi, K. (1965).*Theoretical soil mechanics*. New York: John Wiley & Sons.

Vanmarcke, E. H. (1977). Probabilistic modeling of soil profiles. *Journal of the Geotechnical Engineering Division ASCE* **103**, No. 11, 1227–1246.

Vesić, A. S. (1973). Analysis of ultimate loads of shallow foundations. *Journal of the Soil Mechanics and Foundations Division* **99**, No. 1, 45-73.

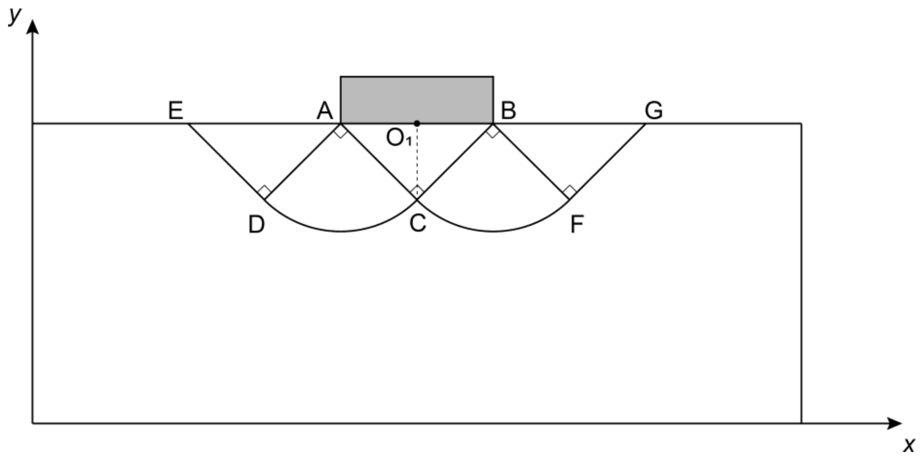


**Fig. 1. Shear failure mechanism in a homogeneous soil**

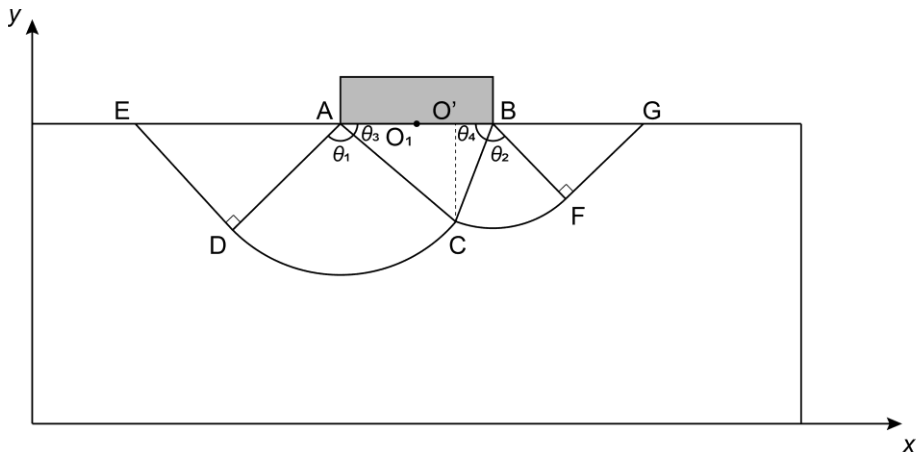


**Fig. 2. Four-parameter variation on shear failure mechanism for spatially variable soil**

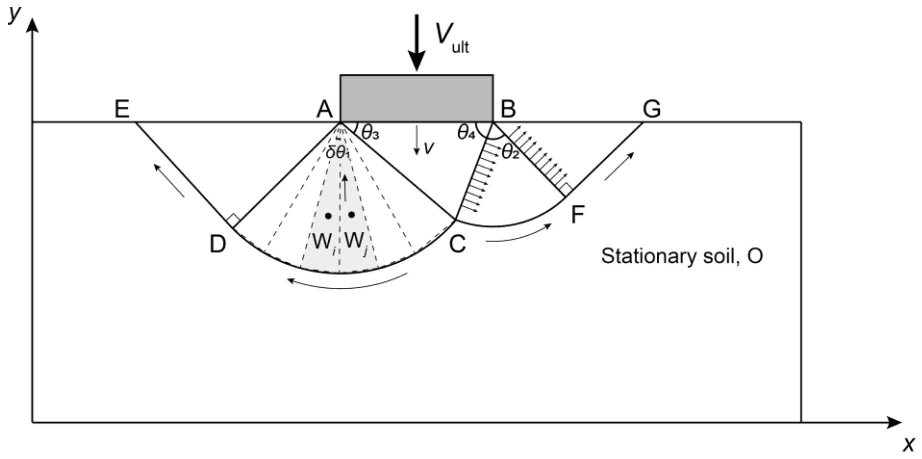


(a)

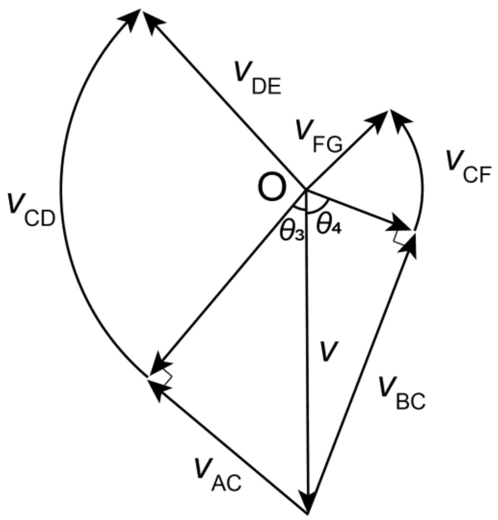


(b)

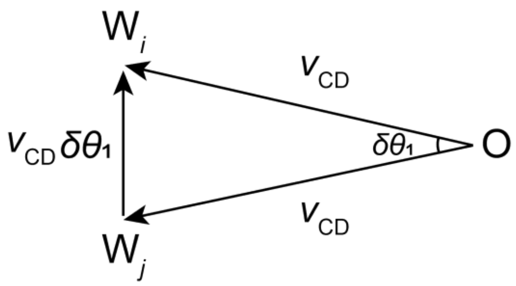


(c)

**Fig. 3. Construction of kinematically admissible velocity field: (a) a potential shear failure mechanism in spatially variable soil; (b) hodograph for spatially variable soil; (c) hodograph for infinitesimal wedge**

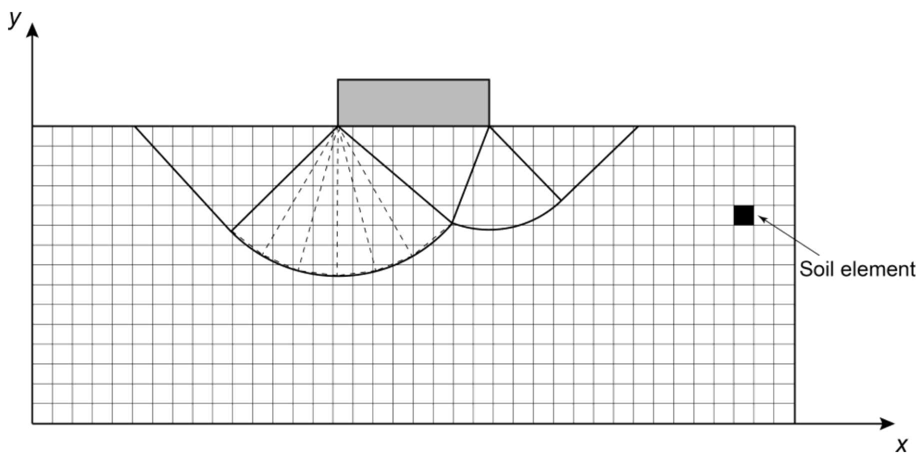


**Fig. 4. Generalized model of a site with spatially variable soil strength**

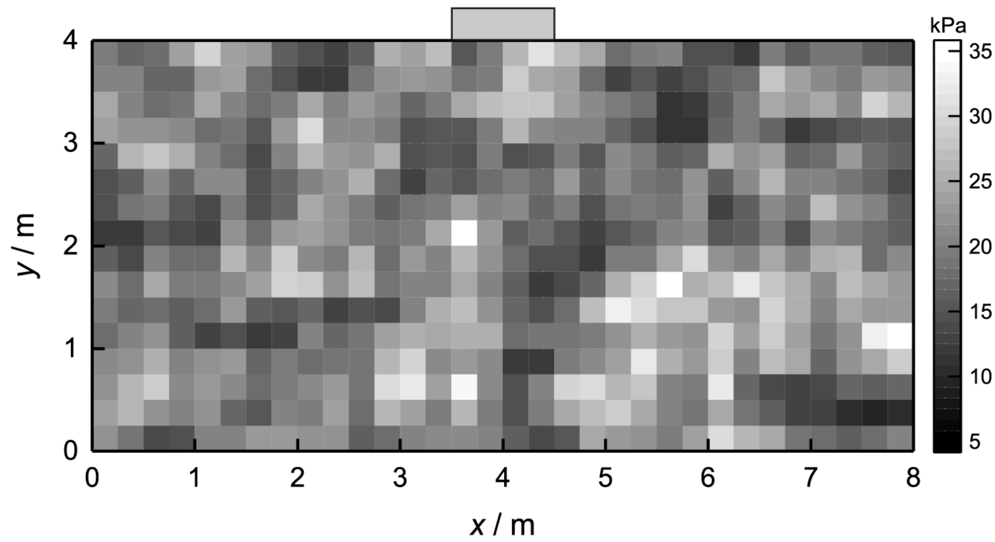


**Fig. 5. Random field of undrained shear strength**

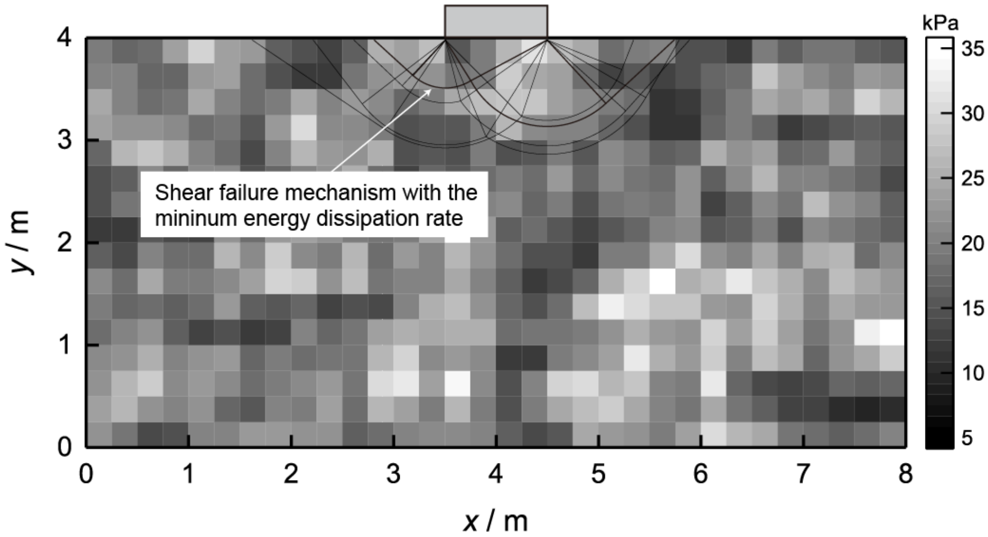


**Fig. 6. Potential shear failure zones**

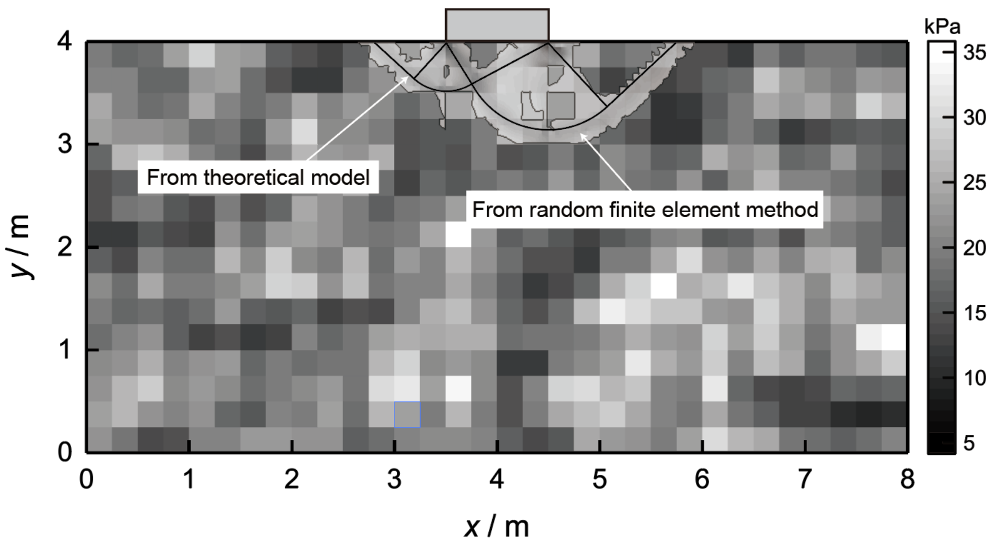


**Fig. 7. Shear failure zones obtained by theoretical model and FEM**

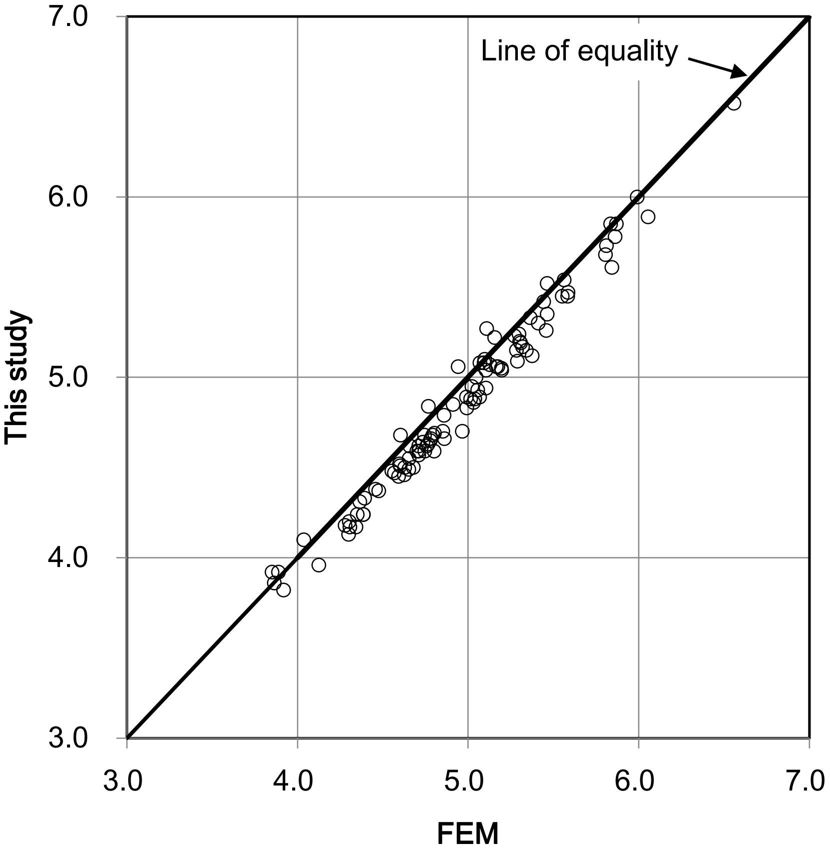


**Fig. 8. Comparison of bearing capacity factors from theoretical model and FEM**

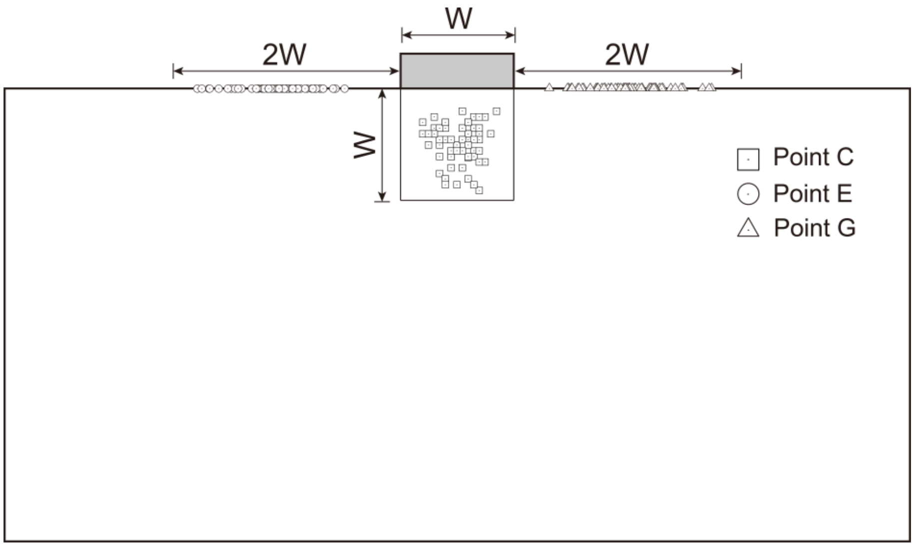


**Fig. 9. Range of control point positions**

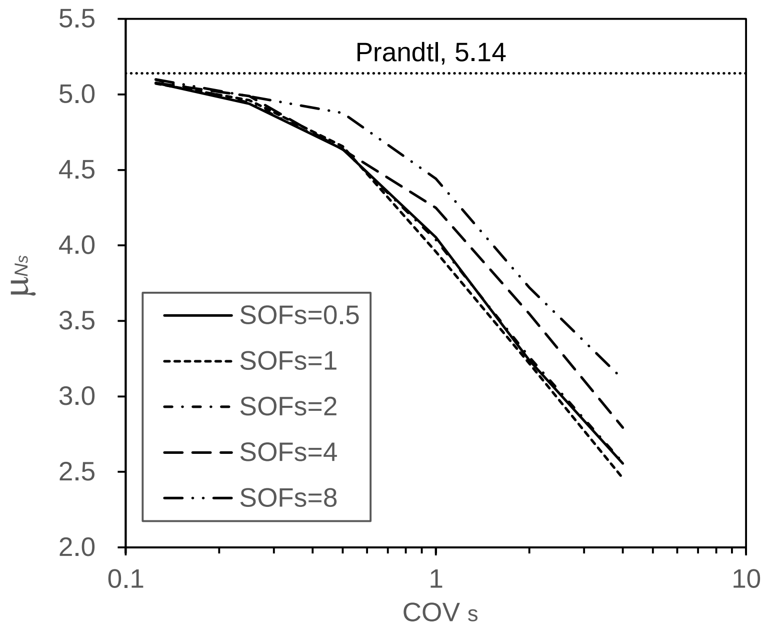


(a)

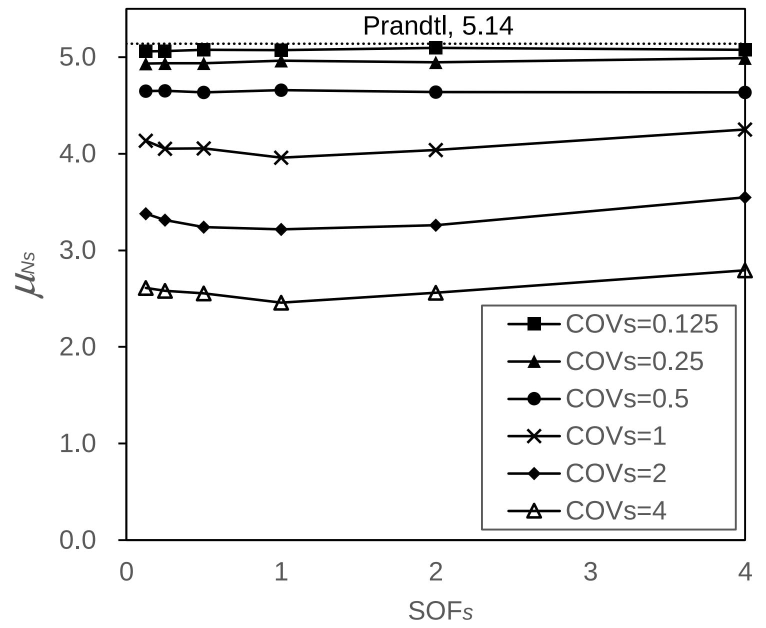


(b)

**Fig. 10. Variation of mean bearing capacity factor with (a) COV of undrained shear strength for different scales of fluctuation; (b) scale of fluctuation for different COV values**

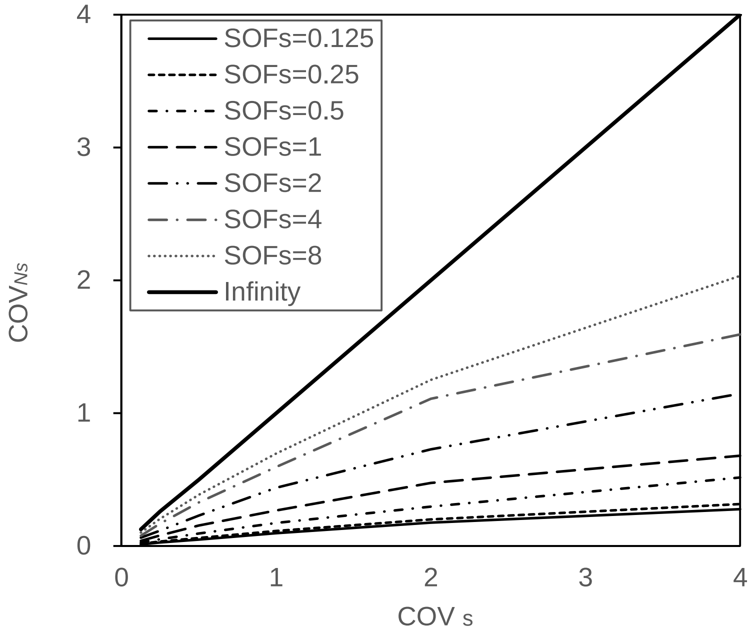


**Fig. 11. Variation of the COV of bearing capacity factor with COV of undrained shear strength for different scales of fluctuation**